Numerical Simulation of Tunnel Fires using preconditioned Finite Volume Schemes

Philipp Birken

September 28, 2006

Philipp Birken
University of Kassel
Department of Mathematics and Computer Science
Heinrich-Plett-Str. 40 (AVZ)
34132 Kassel
Germany
email: birken@mathematik.uni-kassel.de

1

Abstract

This article is concerned with the numerical simulation of flows at low Mach numbers which are subject to the gravitational force and strong heat sources. As a specific example for such flows, a fire event in a car tunnel will be considered in detail. The low Mach flow is treated with a preconditioning technique allowing the computation of unsteady flows, while the source terms for gravitation and heat are incorporated via operator splitting. It is shown that a first order discretization in space is not able to compute the buoyancy forces properly on reasonable grids. The feasibility of the method is demonstrated on several test cases.

Keywords: Preconditioning, Low Mach number flow, Asymptotic analysis, Finite volume method, Conservation laws

1   Introduction

In recent years there were a number of tragic and deadly incidents in car tunnels, for example in the Mont-Blanc tunnel 1999, the Tauern tunnel 1999 or the Kaprun tunnel 2000. This demonstrates the need for more efficient safety measures. There exists a variety of codes designed to provide information on smoke and heat development in buildings, see for example the survey [21].

In praxis, often so called zonal models like the Multi Room Fire Code of Max [14] are applied, which use extremely coarse grids, a division of each cell in hot and cold zones and conservation of mass and energy. These methods are fast and thus allow parameter studies. However, they cannot deal with complicated geometries and provide results that are nonlocal. Furthermore, they are designed for buildings and, due to the missing momentum equation, cannot simulate buoyancy driven flows as those in sloped tunnels.

The alternative to zonal models are so called field models, which correspond to much more accurate tools provided by computational fluid dynamics (CFD). Those can in principal deal with complicated geometries and buoyancy driven flows. The increase in computer power makes the use of these methods applicable to these problems, however there is still need for faster algorithms and faster computers.

The arising flows can be characterized by characteristic speeds of one meter per second and thus a low Mach number ($M \approx 10^{-3}$) and by high temperature gradients. They are driven by buoyancy and the strong heat sources. Caused by these effects, parts of the flow become compressible, although the general situation is nearly compressible. This is similar to a lot of applications, where the Mach number or the compressibility properties vary in time or space. Some examples are nozzle flow, chemically reacting flows or laminar combustion.

In the CFD community, the efficient simulation of low Mach number flows is a subject of ongoing discussion. It is well known that purely compressible flow solvers which were developed for transonic flow fields produce wrong results at low Mach numbers on reasonable

grids and need an unacceptable fine mesh width to provide correct results. This was demonstrated in detail by Volpe [28]. On the other hand, standard incompressible flow solvers cannot deal with strong temperature or strong density gradients. Consequently, there are two main approaches to the design of numerical methods for the above mentioned flows: use either the compressible or the incompressible Euler or Navier-Stokes equations as the basic model and improve upon the existing methods. One important idea in this context was the artificial compressibility method by Chorin [4] that inspired the preconditioner of Turkel [25] for the compressible equations. These methods incorporate a preconditioning of the time derivative of the PDE, thus allowing faster convergence to steady state but sacrificing time accuracy. Along these lines, other preconditioners were proposed [27, 3]. The crucial idea is, that as the Mach number tends to zero, the original system develops a large disparity in wave speeds, as some of the eigenvalues grow to infinity while others remain $\mathcal{O}(1)$. The preconditioner changes all the wave speeds to $\mathcal{O}(1)$, thus greatly improving the condition number of the system.

In this article, we will concentrate on flow solvers which are based on compressible flow. Here, three main techniques to obtain time accuracy can be distinguished. First of all, there is the technique to use the above mentioned preconditioning methods for steady state flows in a pseudo time stepping scheme [24, 26, 29]. Furthermore, there is the flux correction approach, where an approximation to the Euler or Navier-Stokes equations is solved and then corrected via elliptic correction equations [10, 12, 22]. Finally, there is the flux preconditioning approach, where only the dissipation within the numerical flux function of the flow solver is changed by low Mach number preconditioning [9, 18]. This has several advantages. An important one is that the implementation is quite simple. The only part of the flow solver that needs to be changed is the flux function. The other one is that compared to the flux correction approach, the computational effort per time step is smaller.

The addition of source terms is possible in an algorithmically straightforward way using operator splittings. However it turns out, that the new scheme has surprising properties requiring special care in its application.

Besides the low Mach number, the other characterizing property for the tunnel fire problem is the gravitational force, which is responsible for the transport of hot air to the ceiling of the tunnel. A correct computation of the effect of gravitation is thus mandatory for a successful simulation of a tunnel fire event.

Especially in meteorology, flows are considered that are near the hydrostatic balance, meaning that $\partial_{x_2} p - \rho g = \mathcal{O}(\epsilon)$. Several numerical methods exist for these flows, see for example the textbook of Durran [5]. Botta, Klein, Langenberg and Lützenkirchen point out in [2] that some of these methods have problems. If we assume that the solution is near hydrostatic balance, then when discretizing this with mesh width $\Delta x = h$ using a method that is r-th order consistent, we obtain a discretization error of

$$(\partial_{x_2} p - \rho g)_h - \partial_{x_2} p + \rho g = \mathcal{O}(h^r).$$

If ϵ tends to zero while h remains fixed, the discretization error $\mathcal{O}(h^r)$ completely dominates the solution. Thus as we come nearer the hydrostatic equilibrium the quality of the solution does not increase: it is unbalanced. If we know beforehand the correct hydrostatic equilibrium p^H and ρ^H, we have a decomposition $p = \delta p + p^H$ and $\rho = \delta \rho + \rho^H$ satisfying $\partial_{x_2} p^H - \rho^H g = 0$. Then the discretization error for fixed h tends to zero if ϵ tends to zero. However, when using the original discretization without a decomposition, it is not clear from this analysis, how small ϵ can become for a given mesh width and a particular problem, before the discretization error dominates the solution. As a remedy, a reconstruction procedure is suggested in [2], that uses a "discrete Archimedes buoyancy principle" to obtain a well-balanced scheme.

Nguyen-Bui, Dubroca and Maire [20] applied a low Mach preconditioned method to a free convection problem, where air was cooled and heated between plates and, being subject to buoyancy, started to circulate. There they observed errors in their numerical calculations. They tried a similar decomposition of the pressure and could improve their results, though no explanation was given.

The outline of this paper is as follows: In section two, we briefly introduce the model for fire incidents, which consists of the Euler equations of gas dynamics with source terms. Thereafter in section three, a finite volume approximation of the governing equations using a Lax-Friedrichs type scheme is presented whereby we curtly discuss the asymptotic behavior as the Mach number tends to zero. We will then proceed to look closely at the source terms. Here we will use an operator splitting, as this is the simplest thing to do. As the correct resolution of the buoyancy force is crucial, we will first integrate the gravitational source term only. After having examined this by both analysis and numerical experiments we will add heat sources. These are constant in time and space and affect the solution only locally and not globally, as the gravitational term does. Therefore it is much easier to simulate. Finally, we will demonstrate the feasibility of the method by means of several test problems.

2   The governing equations

The Euler equations consist of the conservation laws of mass, momentum and energy, closed by an equation of state. Given an open domain $D \subset \mathbb{R}^2$, the dimensional form can be expressed as

$$\partial_t \mathbf{u} + \sum_{j=1}^{2} \partial_{x_j} \mathbf{f}_j(\mathbf{u}) = \mathbf{g} \quad \text{in } D \times \mathbb{R}^+, \tag{1}$$

where $\mathbf{u} = (\rho, m_1, m_2, \rho E)^T$ represents the vector of conserved variables. The flux functions $\mathbf{f}_j$ and the source term $\mathbf{g}$ are given by

$$\mathbf{f}_j(\mathbf{u}) = \begin{pmatrix} m_j \\ m_j v_1 + \delta_{1j} p \\ m_j v_2 + \delta_{dj} p \\ H m_j \end{pmatrix}, \ j = 1, 2, \ \mathbf{g}(\mathbf{u}) = \begin{pmatrix} 0 \\ \rho g_1 / Fr^2 \\ \rho g_2 / Fr^2 \\ Qq/M^2 \end{pmatrix}$$

4

with δ_{ij} denoting the Kronecker symbol. The quantities ρ, $\mathbf{v} = (v_1, v_2)^T$, $\mathbf{m} = (m_1, m_2)^T$, E and $H = E + \frac{p}{\rho}$ describe the density, velocity, momentum per unit volume, total energy per unit mass and total enthalpy per unit mass, respectively. The pressure is defined by the equation of state for a perfect gas $p = (\gamma - 1)\rho(E - \frac{1}{2}|\mathbf{v}|^2)$, where γ denotes the ratio of specific heats, taken as 1.4 for air.

This form of the Euler equations is obtained by introducing the usual reference values for the length $\hat{x}_{ref}$, the density $\hat{\rho}_{ref}$ and the velocity $\hat{v}_{ref}$. Thus, the non-dimensional characteristic number M appearing in the energy equation is defined as

$$M = \frac{\hat{v}_{ref}}{\hat{c}_{ref}}, \tag{2}$$

where $\hat{c}_{ref} = \sqrt{\hat{p}_{ref}/\hat{\rho}_{ref}}$ denotes the reference value for the speed of sound $\hat{c}$. This reference parameter is related to the Mach number Ma via $M = \sqrt{\gamma}Ma$. Thus, $M = \mathcal{O}_S(Ma)$ and consequently, regarding the asymptotic behaviour with respect to a vanishing Mach number Ma it is of no importance whether Ma or M is used. The other non-dimensional characteristic numbers are the Froude number $Fr = \frac{\hat{v}_{ref}}{\sqrt{\hat{x}_{ref}\hat{g}_{ref}}}$ and the number responsible for the strength of the heatsource $Q = \frac{\hat{q}_{ref}\hat{x}_{ref}}{\hat{p}_{ref}\hat{v}_{ref}}$.

3   Preconditioned Finite Volume Method

Smooth solutions of the Euler equations exist in general only for short times and thus one usually introduces the concept of weak solutions. By means of integrating the system (1) over a control volume Ω and applying Gauss' integral theorem one obtains

$$\frac{d}{dt} \int_{\Omega} \mathbf{u} \, d\mathbf{x} + \sum_{\ell=1}^{2} \int_{\partial\Omega} \mathbf{f}_\ell(\mathbf{u}) n_\ell \, ds = \int_{\Omega_i} \mathbf{g}(\mathbf{u}) d\mathbf{x}, \tag{3}$$

where $\mathbf{n} = (n_1, n_2)^T$ represents the outer unit normal vector on $\partial\Omega$. A mapping $\mathbf{u}$ is called a weak solution of the equations (1) if $\mathbf{u}$ satisfies the integral form of the Euler equations (3) on every bounded set $\Omega \subset D$ which allows to utilize Gauss' integral theorem.

Introducing the cell average $\mathbf{u}_i(t) = \frac{1}{|\Omega_i|} \int_{\Omega_i} \mathbf{u}(\mathbf{x}, t) \, d\mathbf{x}$, the integral form with respect to a polygonally bounded control volume Ω_i can be written as

$$\frac{d}{dt}\mathbf{u}_i(t) = -\frac{1}{|\Omega_i|} \sum_{e_{ij} \subset \partial\Omega_i} \int_{e_{ij}} \sum_{\ell=1}^{2} \mathbf{f}_\ell(\mathbf{u}(\mathbf{x}, t)) n_\ell \, d\mathbf{s} + \frac{1}{|\Omega_i|} \int_{\Omega_i} \mathbf{g}(\mathbf{u}) d\mathbf{x},$$

where e_{ij} denotes the edge between the adjacent control volumes Ω_i and Ω_j.

The convective parts $\mathbf{f}$ and the source terms $\mathbf{g}$, like gravity and heat, will be treated seperately via *fractional step* or *operator splitting* methods. These allow an easy implementation, as they split the solution process in two parts, for both of which well known methods are available. A first order approximation (for smooth solutions $\mathbf{u}$) to this problem is given by

the simple Godunov splitting [8], where we require each "solve" to be at least first order accurate:

1. Solve the Euler equations (1) without the source terms

$$\frac{d}{dt}\mathbf{u}_i(t) + \frac{1}{|\Omega_i|} \sum_{e_{ij} \subset \partial\Omega_i} \int_{e_{ij}} \mathbf{f}(\mathbf{u}(\mathbf{x}, t)) \cdot \mathbf{n} \, d\mathbf{s} = \mathbf{0}, \tag{4}$$

with timestep Δt and initial data $\mathbf{u}^n$ to obtain intermediate data $\mathbf{u}^*$.

2. Solve the ordinary differential equation for heat and gravity

$$\frac{d}{dt}\mathbf{u}_i(t) = \frac{1}{|\Omega_i|} \int_{\Omega_i} \mathbf{g}(\mathbf{x}, t, \mathbf{u}(\mathbf{x}, t)) \, d\mathbf{x}, \tag{5}$$

with the same timestep, but inital data $\mathbf{u}^*$ to obtain $\mathbf{u}^{n+1}$.

In order to evaluate the boundary integral in (4), we employ a numerical flux function of Lax-Friedrichs type

$$H(\mathbf{u}_i, \mathbf{u}_j, \mathbf{n}) = \frac{1}{2}\left(\sum_{\ell=1}^{2} (\mathbf{f}_\ell(\mathbf{u}_i) + \mathbf{f}_\ell(\mathbf{u}_j)) \, n_\ell - \mathbf{D}(\mathbf{u}_i, \mathbf{u}_j, \mathbf{n})(\mathbf{u}_j - \mathbf{u}_i)\right). \tag{6}$$

Numerical methods of this type differ only in the dissipation term $\mathbf{D}$. Hu and Shu [11] defined $\mathbf{D} \in \mathbb{R}$ to be the largest absolute eigenvalue of the corresponding Jacobi matrix

$$\mathbf{F}(\mathbf{u}, \mathbf{n}) = \sum_{\ell=1}^{2} \frac{\partial \mathbf{f}_\ell}{\partial \mathbf{u}_\ell}(\mathbf{u}) n_\ell.$$

Similar to the formulation of Shu and Osher [23] we prefer a matrix-valued term $\mathbf{D}$ which was proposed by Friedrich [6] and afterwards used in [17, 18, 19]. It is proved in [15, 16] that the use of this Lax-Friedrichs-type flux function leads to an unphysical pressure distribution in relevant cases. In particular, variations of the first order pressure field are generated on the space scale $\mathbf{x}$. To extend the validity of the numerical method we utilize a preconditioning technique originally proposed by Guillard and Viozat [9] for the Roe scheme and later on derived in the context of the Lax-Friedrichs method in [18]. Therefore, the dissipation matrix is defined in the sense of $\mathbf{D} = \mathbf{P}^{-1}|\mathbf{PF}|$. In particular, we employ

$$\mathbf{D}(\mathbf{u}_i, \mathbf{u}_j, \mathbf{n}) = \mathbf{P}^{-1}\left(\frac{\mathbf{u}_j + \mathbf{u}_i}{2}\right) \mathbf{R}\left(\frac{\mathbf{u}_j + \mathbf{u}_i}{2}, \mathbf{n}\right) |\mathbf{\Lambda}|(\mathbf{u}_i, \mathbf{u}_j, \mathbf{n}) \mathbf{R}^{-1}\left(\frac{\mathbf{u}_j + \mathbf{u}_i}{2}, \mathbf{n}\right).$$

Herein, $\mathbf{R}(\mathbf{u}, \mathbf{n})$ represents the matrix of the right eigenvectors of the corresponding preconditioned Jacobian

$$\mathbf{F}^P(\mathbf{u}, \mathbf{n}) = \mathbf{P}(\mathbf{u})\mathbf{F}(\mathbf{u}, \mathbf{n})$$

and $|\mathbf{\Lambda}|(\mathbf{u}_i, \mathbf{u}_j, \mathbf{n})$ denotes the diagonal matrix defined by

$$|\mathbf{\Lambda}|(\mathbf{u}_i, \mathbf{u}_j, \mathbf{n}) = \text{diag}\left\{\max_{\mathbf{u} \in \left\{\mathbf{u}_i, \mathbf{u}_j, \frac{\mathbf{u}_i + \mathbf{u}_j}{2}\right\}} |\lambda_1(\mathbf{u}, \mathbf{n})|, \ldots, \max_{\mathbf{u} \in \left\{\mathbf{u}_i, \mathbf{u}_j, \frac{\mathbf{u}_i + \mathbf{u}_j}{2}\right\}} |\lambda_4(\mathbf{u}, \mathbf{n})|\right\},$$

where $\lambda_i(\mathbf{u}, \mathbf{n})$, $i = 1, \ldots, 4$ are chosen to be the eigenvalues of the matrix $\mathbf{F}^P(\mathbf{u}, \mathbf{n})$. The properties of the derived method strongly depend on the preconditioning matrix used. Arranging $\mathbf{P}(\mathbf{u}, \mathbf{n})$ to be the identity yields the Lax-Friedrichs-type scheme including a matrix-valued local dissipation term proposed by Friedrich [6]. In order to overcome the failure of the standard Lax-Friedrichs scheme with respect to the pressure distribution in the low Mach number regime it is quite natural to multiply the pressure by a factor associated with the Mach number. Therefore, we extract the pressure by consideration of the so-called entropy variables $\mathbf{w} = (p, v_1, v_2, s)^T$, whereby s denotes the entropy determined as $s = \ln \frac{p}{\rho^\gamma}$. Following Turkel [25] we introduce

$$\mathbf{P}(\mathbf{u}) = (\mathbf{UQW})(\mathbf{u}), \tag{7}$$

where $\mathbf{U} = \frac{\partial \mathbf{u}}{\partial \mathbf{w}}$, $\mathbf{W} = \frac{\partial \mathbf{w}}{\partial \mathbf{u}}$ and

$$\mathbf{Q} = \begin{pmatrix} \beta^2 & 0 & 0 & 0 \\ 0 & 1 & 0 & 0 \\ 0 & 0 & 1 & 0 \\ 0 & 0 & 0 & 1 \end{pmatrix}, \text{ with } \beta = \mathcal{O}_S(M), \ M \to 0. \tag{8}$$

To ensure that the matrix is always nonsingular we additionally require that $\beta \neq 0$ for all $M > 0$. Simple but time-consuming calculations give

$$\mathbf{P}(\mathbf{u}) = \mathbf{I} + \frac{\gamma - 1}{c^2}(\beta^2 - 1) \begin{pmatrix} \frac{|v|^2}{2} & -v_1 & -v_2 & 1 \\ \frac{|v|^2 v_1}{2} & -v_1^2 & -v_1 v_2 & v_1 \\ \frac{|v|^2 v_2}{2} & -v_1 v_2 & -v_2^2 & v_2 \\ \frac{|v|^2 H}{2} & -Hv_1 & -Hv_2 & H \end{pmatrix}$$

and

$$\lambda_{1,2}(\mathbf{u}, \mathbf{n}) = v_{\mathbf{n}} := \mathbf{v} \cdot \mathbf{n},$$
$$\lambda_{3,4}(\mathbf{u}, \mathbf{n}) = \frac{1}{2}\left[(1 + \beta^2)v_{\mathbf{n}} \pm \sqrt{(1 + \beta^2)^2 v_{\mathbf{n}}^2 - 4v_{\mathbf{n}}^2\beta^2 + 4\beta^2 c^2}\right].$$

It was recently proven in [15] that utilizing the preconditioned Lax-Friedrichs flux (6) for the choice (8), within the finite volume method associated with (4) yields a pressure distribution satisfying the asymptotic properties of the continuous equations in a discrete sense. Furthermore, a discrete divergence constraint corresponding to the results known for the continuous equations is shown for this scheme in [19] in the absence of compression and expansion over the boundary of the computational domain.

As was shown in [1], the preconditioned method combined with an explicit time integration has unfavorable stability properties. More precise, the time step has to go to zero with $\mathcal{O}(M^2)$ as the Mach number tends to zero. Therefore, implicit methods are to be favored.

4   A First Test Case

To analyze the behavior of our methods for flows subject to a buoyant force, we consider a two dimensional longitudal section of a tunnel of five meter height with the bottom of

the tunnel being at zero altitude. For the velocity we use the initial data $v_1 = const = 1$ and $v_2 = const = 0$. We choose a pressure and density distribution which varies only in horizontal direction, such that the gravitational force term is balanced out by the pressure gradient. Thus we choose $p(x_2)$ and $\rho(x_2)$ according to the hydrostatic pressure:

$$p(x_2) = p_r \left(1 - \frac{\Gamma x_2}{T_r} \right)^{c_p/R}. \tag{9}$$

Thus, the pressure decays at a very small rate due to the height of a tunnel and is nearly linear in x_2. The density distribution is also a function of height:

$$\rho(x_2) = \frac{p_r}{RT_r} \left(1 - \frac{\Gamma x_2}{T_r} \right)^{c_p/R - 1}. \tag{10}$$

For the discrete initial data, we use the above formula to determine pressure and density in the cell centers, which results in no variations in x_1-direction. For a reference pressure of 101325 Pa, we obtain an exact pressure difference from top to bottom of 63,4 Pa and a Mach number of $Ma = 0.0036$. Thus, the initial data corresponds approximately to a steady state. Approximately only, because the discrete equations have a slightly different steady state than the continuous equations. Nevertheless, the physical flux of the flow should balance with the gravitational force and there should be almost no energy flux in x_2-direction. The ϵ from the introduction is in this example zero, because we are exactly in hydrostatic balance. Thus the discretization error can be seen very well. We will use a cartesian grid with quadratic cells, where we employ twenty cells in x_2-direction.

4.1 Numerical Experiments

Tom compute the steady state, we use a first order discretization in space and the explicit Euler method in time, despite the bad stability properties to eliminate possible influences from errors of the inner iterations. At the tunnel ends, Neumann boundary conditions are used.

For the first run, we use the unpreconditioned Lax-Friedrichs flux and a CFL number of 0.9. The solution after 5000 time steps is already a steady state. A correct nearly linear distribution of the density is obtained and the pressure distribution changes slightly, while preserving the pressure difference of 63,4 Pa. This is probably due to the coarse grid and the fact that the discretization is only of first order.

The second run is done using the low Mach preconditioned Lax-Friedrichs flux. Here, also a nearly linear distribution of the density is obtained, but the pressure difference from top to bottom reduces to three Pascal after 5000 time steps with a CFL number of 0.0036. Then it increases slowly. After 100.000 time steps, a pressure difference of 54 Pa is obtained.

8

The unpreconditioned method thus produces a physically reasonable result, while the preconditioned method does not. To illustrate the problem, we repeat the experiment, but this time, only one time step of the flow solver without source terms is performed in both cases. For a cell in the middle of the tunnel, we obtain the following conservative fluxes:

Component	Preconditioned	Unpreconditioned
ρ	$1.58499 \cdot 10E - 10$	$1.88016 \cdot 10E - 8$
ρv_1	$1.58499 \cdot 10E - 10$	$1.88016 \cdot 10E - 8$
ρv_2	-0.324404	-0.324404
ρE	-1.83711	-0.0034101

The physical flux update in the first step is $\mathbf{f} = (0, 0, \Delta p, 0)^T$. The energy flux in both cases is thus too big, but much worse so in the preconditioned case.

4.2 Analysis of the Energy Flux

To understand this phenomenon, we look at the flux updates in an interior cell in the first step. The fluxes in x_1-direction cancel out, but along horizontal borders they differ and therefore the reason for the above demonstrated behavior must lie in the horizontal flux. We have for the preconditioned flux function with $\mathbf{n} = (0, 1)^T$:

$$\mathbf{f}^{LFP}(\mathbf{u}_L, \mathbf{u}_R; \mathbf{n}) = \frac{1}{2}(\mathbf{f}_L + \mathbf{f}_R - \mathbf{D}\Delta\mathbf{u}) = \frac{1}{2}(\begin{pmatrix} 0 \\ 0 \\ 2p \\ 0 \end{pmatrix} - \mathbf{D} \begin{pmatrix} \Delta\rho \\ \Delta\rho \cdot v_1 \\ 0 \\ \Delta E \end{pmatrix}).$$

The unpreconditioned flux is the same, though with a different dissipation matrix $\check{\mathbf{D}}$. The energy component we are interested in depends only on the dissipation term and we obtain for the preconditioned case, using the abbreviations $\xi_1 = \lambda_3 - \beta^2 v_n$, $\xi_2 = \lambda_4 - \beta^2 v_n$ and $\xi_3 = \frac{\lambda_4 - \lambda_3}{2}$:

$$
\begin{aligned}
\mathbf{D}_4\Delta\mathbf{u} &= |\lambda_1|\frac{|\mathbf{v}|^2}{2}\left\{(1 - \frac{(\gamma-1)|\mathbf{v}|^2}{2c^2})\Delta\rho + \frac{\gamma-1}{c^2}v_1(\Delta\rho v_2) + \frac{\gamma-1}{c^2}v_2\Delta(\rho v_2)\right. \\
&\quad \left. - \frac{\gamma-1}{c^2}\Delta(\rho E)\right\} \\
&\quad - |\lambda_2|v_t[v_t\Delta\rho + n_2\Delta(\rho v_1) - n_1\Delta(\rho v_2)] \\
&\quad + \frac{1}{2\beta^2 c^2 \xi_3}\left\{|\lambda_3|(H + \xi_1 v_n)\left[(\xi_2(\gamma-1)\frac{|\mathbf{v}|^2}{2} + \beta^2 c^2 v_n)\Delta\rho\right.\right. \\
&\quad \left.\left. - (\xi_2(\gamma-1)v_1 + \beta^2 c^2 n_1)\Delta(\rho v_1) - (\xi_2(\gamma-1)v_2 + \beta^2 c^2 n_2)\Delta(\rho v_2)\right.\right.
\end{aligned}
$$

9

$$+ (\gamma - 1)\xi_2 \Delta(\rho E)\Big]$$

$$+ |\lambda_4|(H + \xi_2 v_n)\Big[-(\xi_1(\gamma - 1)\frac{|\mathbf{v}|^2}{2} + \beta^2 c^2 v_n)\Delta\rho$$

$$+ (\xi_1(\gamma - 1)v_1 + \beta^2 c^2 n_1)\Delta(\rho v_1) + (\xi_1(\gamma - 1)v_2 + \beta^2 c^2 n_2)\Delta(\rho v_2)$$

$$- (\gamma - 1)\xi_1 \Delta(\rho E)\Big]\Big\}.$$

In this testcase, we have $v_n = v_2 = 0$ and thus, $\lambda_1 = \lambda_2 = 0$, as well as $\Delta(\rho v_2) = 0$. Thus, using that we furthermore have $|\lambda_4| = |\lambda_3| = \beta c$ and $\xi_2 - \xi_1 = 2\xi_3$, straightforward computations lead to

$$f_4^{LFP} = \mathbf{D}_4 \Delta\mathbf{u} = \frac{H(\gamma - 1)}{\beta c}\left(\frac{|\mathbf{v}|^2}{2}\Delta\rho + v_1\Delta(\rho v_1) + \Delta(\rho E)\right). \tag{11}$$

In the unpreconditioned case $\beta = 1$ the formula for the flux simplifies to:

$$f_4^{LF} = \check{\mathbf{D}}_4 \Delta\mathbf{u} = \frac{H(\gamma - 1)}{c}\left(\frac{|\mathbf{v}|^2}{2}\Delta\rho + v_1\Delta(\rho v_1) + \Delta(\rho E)\right). \tag{12}$$

Thus, the vertical fluxes differ by a factor of $1/\beta$. The update of a nonboundary cell is formed by the difference between the flux from the top of the cell and the flux from the bottom of the cell, as the numerical solution does not vary in x_1-direction. The update is though even in this simple testcase a complicated nonlinear function of the initial data. Nevertheless, we can deduct an asymptotic behavior. The total energy per unit volume E and the total enthalpy per unit volume H are $\mathcal{O}(M^{-2})$. Thus, for a given initial pressure and density distribution in x_2-direction, we expect the update in the preconditioned case to increase of fourth order with the Mach number going to zero and in the unpreconditioned of third order. This can indeed be confirmed by numerical results. The tables show the energy flux update in an interior cell for the test problem at different Mach numbers.

Mach number	0.1	0.01	0.001	0.0001	0.00001
Prec. flux	0.001270	122.9158	1229132	12291317684	$1.2291317658 \cdot 10E14$
Unprec. flux	0.001270	1.267485	1267.459	1267458.88783	1267458885.15

Vertical energy flux using a first order discretization at different Mach numbers

The flux behaves as predicted for Mach numbers smaller than 0.1, for higher Mach numbers the $\mathcal{O}(1)$ terms influence the flux. This effect of increasing flux can lead to steady states where the balance between the preconditioned flux and the gravitational source term is achieved at a very small and unphysical pressure difference. There are two ways to remedy this, as can be seen from (11). We can decrease the last factor and thereby the flux by decreasing the differences in the data either by refining the mesh or by using a method of

higher order in space. In the same test case as above but using MUSCLE interpolation, the energy flux can be significantly decreased. This is demonstrated in the following tabular.

Mach number	0.1	0.01	0.001	0.0001	0.00001
Prec. flux	$7.88449 \cdot 10E - 9$	0.000854110	8.54112	85411.2	854111161
Unprec. flux	$7.88449 \cdot 10E - 9$	$8.80744 \cdot 10E - 6$	0.00880745	8.80745	8807.44

Vertical energy flux using a higher order discretization at different Mach numbers

The dependence on the Mach number is as in the first case and as predicted by the analysis, but the size of the flux is decreased by a factor of 10^6, which allows to compute the correct pressure distribution up to an error of a few Pascal for moderately small Mach numbers. For $M = 10^{-5}$ a refinement of the grid is necessary, despite the higher order. Nevertheless, the results show that a pressure splitting as suggested in the introduction is not necessary to compute a correct pressure distribution.

The reason for this is probably, that a linear pressure distribution is globally a very good approximation for the pressure field in a tunnel of five or ten meter height where one cell corresponds to about 25 cm. Thus the higher order method, which uses a linear representation in every cell has a very small discretization error in comparison to the first order method. For the meteorological problems considered by Botta, Klein, Langenberg and Lützenkirchen, where the height is on a scale of several kilometers and one cell is of the scale of dozens of meters, the pressure is truly nonlinear and this statement is no longer true.

Recently, Lee [13] demonstrated that for the here employed low Mach preconditioning techniques, the convergence rate towards the steady state is slowest in the energy equation and gets worse the smaller the Mach number. More, the convergence rate in the mass and momentum equations was not affected by the preconditioning. We believe that the above results are a pointer to why this is so.

5   Gravitation and a Heat Source

Having demonstrated that the preconditioned method is able to solve problems with gravitation, we now look at both gravitation and a heat source together. We skip the case where only the heat source is active, as this does not lead to interesting test cases.

First we compute the steady state in a short tunnel with two sharp bends. It starts level for six meters, then proceeds for 14 meters with a three % slope and continues again flat for another six meters. For the initial data, we use hydrostatic pressure and and a Mach number of 0.01. In the initial velocity field, the vertical component is set to zero. Then we compute the steady state. Finally, a circular package of heat is placed near the entrance of the tunnel. The initial temperature in the hot zone is up to 450 Kelvin, as can be seen
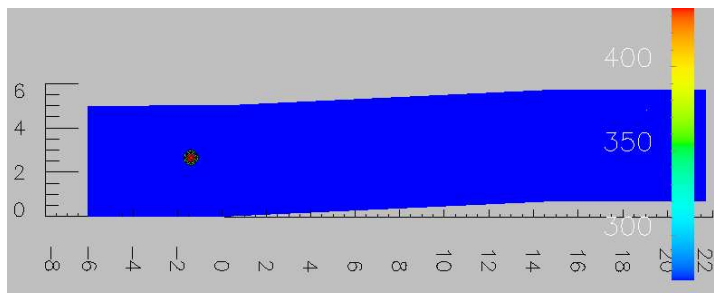
Figure 1: Initial position of the package of heat in the bended tunnel
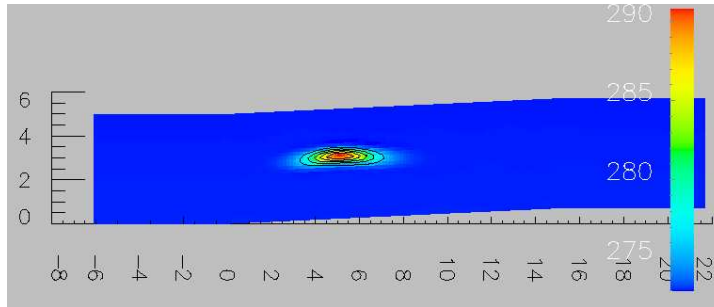

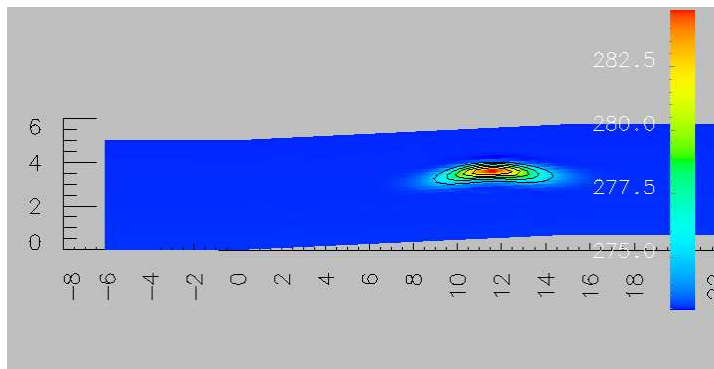
Figure 2: Temperature distribution after 1.9 seconds

Figure 3: Temperature distribution after 3.7 seconds

in figure 5. After 1.9 seconds, the package has moved with the flow about seven meters to the beginning of the slope and a bit upwards. The heat is distributed over a larger area with a temperature of 290 Kelvin in the hottest cell. Figure 1 shows that the package is no longer circular, but drawn out to the ceiling. After 3.7 seconds, the package has reached the second bend, which can be seen in figure 2. It is now more boomerang shaped, because the hottest air with a peak temperature of 285 Kelvin is in the center and flows toward the ceiling faster than the cooler parts of the package. This is what was expected to happen and thus we move on to fire events.

5.1 Simulation of a Fire Event

The final test case is similar to a fire event with a burning vehicle in the middle of a tunnel. We use a rectangular heat source of the size $3m \times 5m$, thus ranging from bottom to top of the tunnel. It is placed in the middle of a tunnel which is one kilometer long and has no slope. At the boundary, we prescribe the hydrostatic pressure (9). The initial conditions are obtained by first computing the steady state if the heat source is not active.

We will perform two runs with different fires with a total power of ten MW and one MW. If we assume that the tunnel is ten meters wide, the heat source is distributed over a volume of $150m^3$ and we have to divide the total power by this to obtain the proper $\hat{q}_{ref}$. With an inflow Mach number of $Ma = 0.01$ this leads to a nondimensional parameter Q of 32350 and 3235, respectively, and the Froud number for a reference length of $\hat{x}_{ref} = 5m$ is $Fr = 0.488$. The grid we use is cartesian with 32×464 cells. These are smallest and quadratic in the middle of the tunnel and become thinner towards the exit, up to an aspect ratio of 1:16. This setting is similar to that described in [7], however there the fire is distributed over a volume of $400m^3$ and thus the power per unit volume is smaller.

The simulations run until five seconds of realtime are reached. For the time integration of the Euler equations we use the implicit midpoint rule. Up to three Newton steps are performed in every time step. Fewer steps are performed, if the euclidian norm of the relative nonlinear residual has dropped by a factor of 100 before. If this nonlinear tolerance was set to a factor of 10, divergence could happen. We start with a CFL number of 0.01, which is increased if fewer than three Newton steps were needed, up to a CFL number of 1.5. As for the linear equation systems, they are solved until the euclidian norm of the relative linear residual has dropped by a factor of 10^5.

5.2 Description of the Results for the Fire Events

The pictures 4 up to 12 show the middle part of the tunnel at different times during the fire event. It can be clearly seen that the heat concentrates on the ceiling, due to the buoyancy. Furthermore, it slowly drifts downstream, at about the rate of 3.6 m/s. A circulation of the flow, generated by hot air moving upwards can be seen in all cases in the velocity profiles or the Mach number distribution. Looking at the flow to the left and right of the fire, we see that the fire acts as a sort of wall for the flow. Downstream, the flow velocity decreases, but increases upstream. Another observation is that the speed of sound increases locally. This can be explained by the heat source: Additional heat leads to a boost in the internal energy, which is connected to the pressure, but not the total mass, and thus the speed of sound $c = \sqrt{\gamma \frac{p}{\rho}}$ is increased. This is bad for the time integration, because for a constant CFL number, an increase in the speed of sound leads to smaller time steps. In the case of the ten megawatt fire, this leads to a time step at five seconds, which is nearly ten times smaller than the time step at the beginning.

After five seconds of the one MW fire event, the temperature has increased by about 30 Kelvin. To the left of the fire, the temperature isolines are almost vertical, to the right the
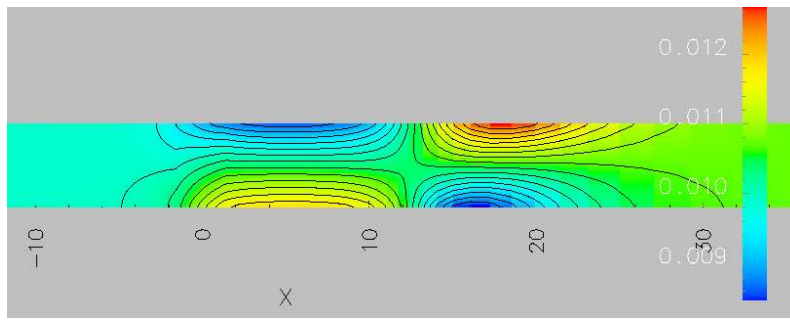
13

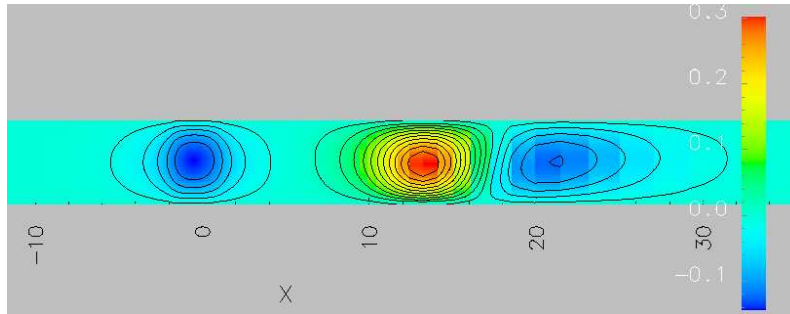Figure 4: Mach number for 1 MW after 5 seconds

Figure 5: Horizontal velocity for 1 MW after 5 seconds
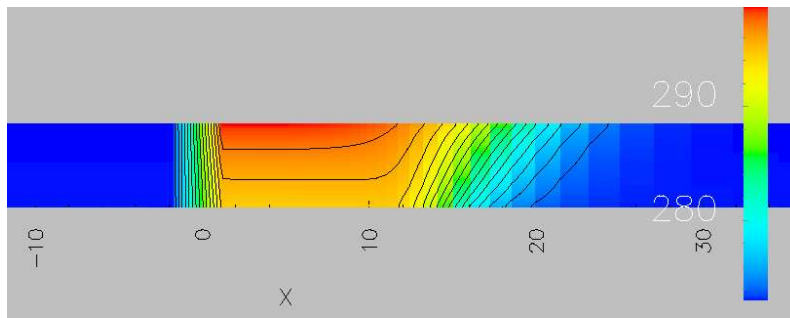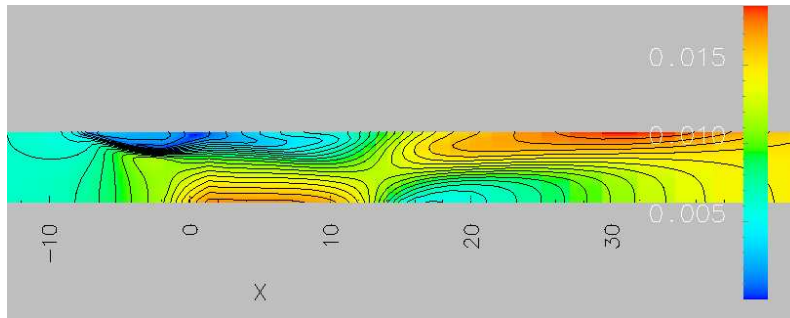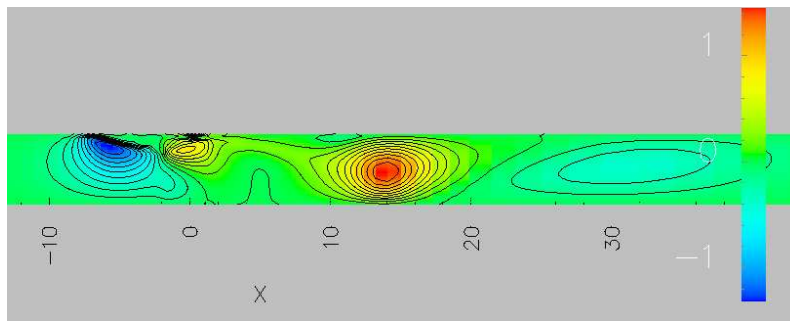

Figure 6: Temperature for 1 MW after 5 seconds

heat propagation concentrates near the cealing. An effect of the fire can be observed up to twenty meters downstream, which coincides with the flow velocity.

For the ten MW fire, the increase in temperature is immense, actually several thousand Kelvin, in one single cell it is up to 14.000 Kelvin. However, this extreme heat is only in the top layer of cells. In the cells in the line next to the top, the temperature is between seven and eight tousand Kelvin and two meters away from the ceiling, directly in the area of the heat source, the temperature is less than one tousand Kelvin. Near the ceiling, there is a propagation of heat in upstream direction which leads to a strong shock. This is probably due to the extreme temperature gradients which leads to large pressure gradients which cause the air to move upstreams. Thus it can be observed, that the flow is absolutely not incompressible. To the right, the hot air has propagated up to 40 m.

The linear equation systems are hard to solve. Already for CFL numbers around 0.5, a

100 GMRES iterations and more are needed. The computation takes about three days on a one GHz Pentium to compute one second of realtime. This is due to the large number of GMRES iterations: if three Newton steps are needed, as was usually the case, about 300 GMRES iterations are performed. The problem is thus significantly more difficult to solve than for the scenarios with less powerful fires, both for the nonlinear and the linear equations systems. It is also quite clear that the method is much too slow to be applied in practice, where the goal is to perform parameter studies on a PC.

Figure 7: Mach number for 10 MW after 5 seconds

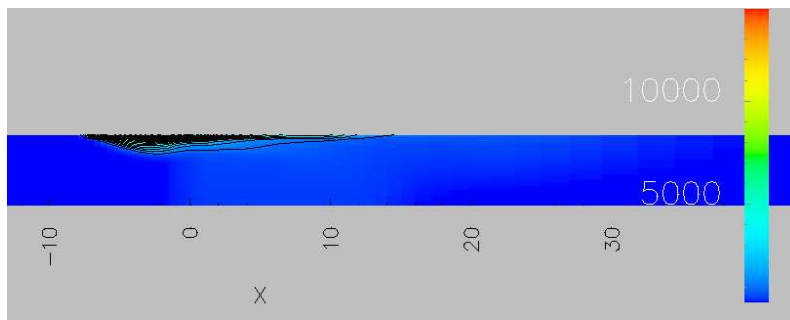Figure 8: Horizontal velocity for 10 MW after 5 seconds

Figure 9: Temperature for 10 MW after 5 seconds

A computation on a longer time scale is shown in figures 10 to 12. The one MW tunnel fire was computed beyond the five seconds, up to sixty seconds real time. The heat does not increase significantly anymore, and the propagation of heat downstream is according to the basic flow velocity. The air circulates between bottom and ceiling, but in a steady way. This can also be seen in the nonlinear equation systems, where now one or at most two Newton steps are sufficient.
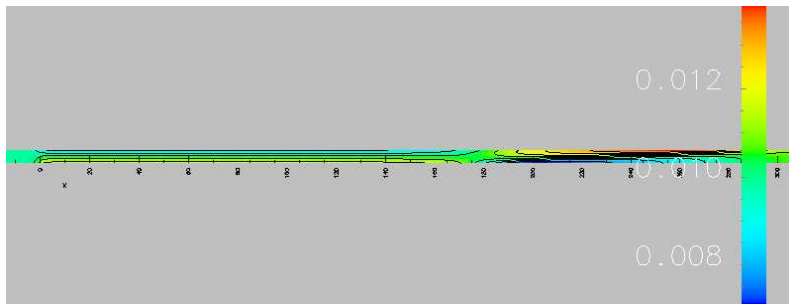
15

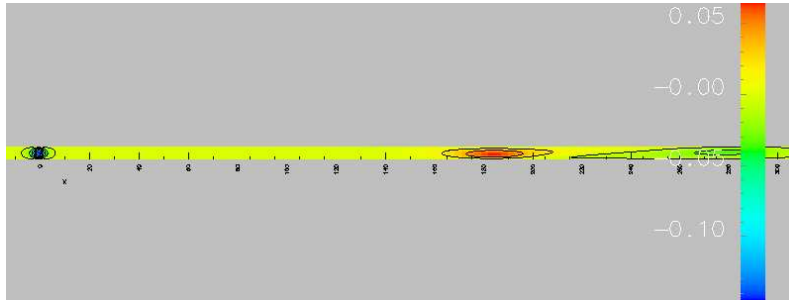Figure 10: Mach number for 1 MW after 60 seconds

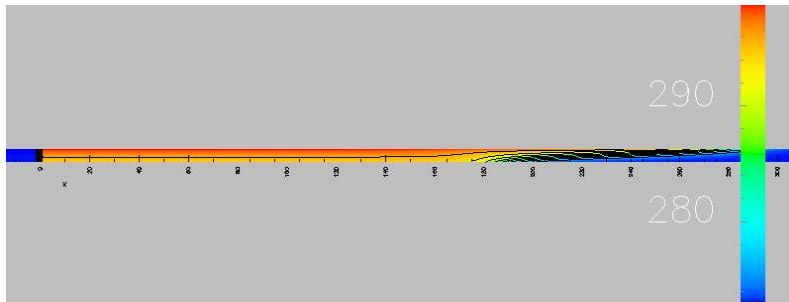Figure 11: Horizontal velocity for 1 MW after 60 seconds

Figure 12: Temperature for 1 MW after 60 seconds

6   Conclusions

It was shown that a first order discretization in space is not able to resolve buoyancy on reasonable grids. A higher order method combined with a low Mach number preconditioned finite volume method produces results that are in agreement with physics as far as we can tell. In all cases the heat gets transported to the ceiling and propagates fastest down-stream, where the additional kinetic energy through the fire leads to a significantly faster propagation for the stronger heat source. The pressure field is in line with the expectations.

Acknowledgments

References

[1] P. BIRKEN AND A. MEISTER, *Stability of Preconditioned Finite Volume Schemes at Low Mach Numbers*, BIT, 45(3) (2005). accepted.

[2] N. BOTTA, R. KLEIN, S. LANGENBERG, AND S. LÜTZENKIRCHEN, *Well balanced finite volume methods for nearly hydrostatic flows*, J. Comput. Phys., 196 (2004), pp. 539–565.

[3] D. CHOI AND C. L. MERKLE, *The Application of Preconditioning in Viscous Flows*, J. Comput. Phys., 105 (1993), pp. 207–223.

[4] A. J. CHORIN, *A Numerical Method for Solving Incompressible Viscous Flow Problems*, J. Comput. Phys., 2 (1967), pp. 12–26.

[5] D. DURRAN, *Numerical Methods for Wave Equations in Geophysical Fluid Dynamics*, Springer, New York, 1999.

[6] O. FRIEDRICH, *Weighted Essential Non-Oscillatory Schemes for the Interpolation of Mean Values on Unstructured Grids*, J. Comput. Phys., 144 (1998), pp. 194–212.

[7] I. GASSER, J. STRUCKMEIER, AND I. TELEAGA, *Modelling and Simulation of Fires in Vehicle Tunnels*, Int. J. for Numerical Methods in Fluids, 44 (3) (2004), pp. 277–296.

[8] S. K. GODUNOV, *A Finite Difference Method for the Numerical Computation of Discontinuous Solutions of the Equations of Fluid Dynamics*, Mat. Sb., 47 (1959), pp. 357–393.

[9] H. GUILLARD AND C. VIOZAT, *On the Behaviour of Upwind Schemes in the Low Mach Number Limit*, Computers and Fluids, Vol. 28 (1999), pp. 63–86.

[10] L. HOFFMANN AND A. MEISTER, *A Compressible Low Mach Number Scheme based on Image Processing and Asymptotic Analysis*, Computational Fluid Dynamics Journal, Vol. 9 (2001), pp. 231–242.

[11] C. HU AND C. SHU, *Weighted Essentially Non-oscillatory Schemes on Triangular Meshes*, J. Comput. Phys., 150 (1999), pp. 97–127.

[12] R. KLEIN, N. BOTTA, T. SCHNEIDER, C. MUNZ, S. ROLLER, A. MEISTER, L. HOFFMANN, AND T. SONAR, *Asymptotic adaptive methods for multi-scale problems in fluid mechanics*, Journal of Engineering Mathematics, Vol. 9 (1/4) (2001), pp. 261–343.

[13] S.-H. LEE, *Convergence characteristics of preconditioned euler equations*, J. Comp. Phys., 208 (2005), pp. 266–288.

[14] U. MAX, *Zur Berechnung der Ausbreitung von Feuer und Rauch in komplexen Gebäuden*, PhD thesis, University of Kassel, 1990.

[15] A. MEISTER, *Analyse und Anwendung Asymptotik-basierter numerischer Verfahren zur Simulation reibungsbehafteter Strömungen in allen Mach-Zahlbereichen*, Habilitation, Universität Hamburg, 2001.

[16] ———, *Theoretical investigation of the Lax-Friedrichs scheme in the low Mach number limit*, in Discrete Modelling and Discrete Algorithms in Continuum Mechanics, Berlin, 2001, Logos Verlag, pp. 177–186.

[17] ———, *Asymptotic Expansions and Numerical Methods in Computational Fluid Dynamics*, in Industrial Mathematics and Statistics, J. C. Misra and et. al., eds., New Delhi, 2002.

[18] ———, *Asymptotic based preconditioning technique for low Mach number flows*, Z. Angew. Math. Mech., 83 (2003), pp. 3–25.

[19] ———, *Viscous Flow Fields at all Speeds: Analysis and Numerical Simulation*, Journal of Applied Mathematics and Physics (ZAMP), 54 (2003), pp. 1010–1049.

[20] N.-H. NGUYEN-BUI, B. DUBROCA, AND P.-H. MAIRE, *Application of turkel preconditioned method in external free convection and incompressible flows*, in Conference on Mathematical and Numerical Aspects of Low Mach Number Flows, 2004.

[21] S. M. OLENICK AND D. J. CARPENTER, *An Updated International Survey of Computer Models for Fire and Smoke*, J. of Fire Protection Engineering, 13 (2003), pp. 87–110.

[22] T. SCHNEIDER, N. BOTTA, K. J. GERATZ, AND R. KLEIN, *Semi-Implicit Extension of a Godunov-Type Compressible Solver Based on Low Mach Number Asymptotics II: Multi-Dimesional, Variable Density Zero Mach Number Flow*, J. Comput. Phys., 155 (1999), pp. 248–286.

[23] C. SHU AND S. OSHER, *Efficient Implementation of Essentially Nonoscillatory Shock-Capturing Schemes*, J. Comput. Phys., 77 (1988), pp. 439–471.

[24] J.-S. SHUEN, K.-H. CHEN, AND Y. CHOI, *A Coupled Implicit Method for Chemical Non-equilibrium Flows at All Speeds*, J. Comput. Phys., 106 (1993), pp. 306–318.

[25] E. TURKEL, *Preconditioned Methods for Solving the Incompressible and Low Speed Compressible Equations*, J. Comput. Phys., 72 (1987), pp. 277–298.

[26] E. TURKEL AND V. VATSA, *Choice of Variables and Preconditioning for Time Dependent problems*, AIAA Paper, 2003-3692 CP (2003). AIAA 16th Computational Fluid Dynamics Conference, Orlando.

[27] B. VAN LEER, W.-T. LEE, AND P. ROE, *Characteristic Time-Stepping or Local Preconditioning of the Euler Equations*, AIAA Paper, AIAA-91-1552 (1991).

[28] G. VOLPE, *Performance of Compressible Flow Codes at Low Mach Numbers*, AIAA J., 31 (1993), pp. 49–56.

[29] J. M. Weiss and W. A. Smith, *Preconditioning Applied to Variable and Constant Density Flows*, AIAA J., 33 (1995), pp. 2050–2057.